



Lab on a Chip

Deciphering Fibroblast-Induced Drug Resistance in Non-Small Cell Lung Carcinoma through Patient-Derived Organoids in Agarose Microwells

Journal:	<i>Lab on a Chip</i>
Manuscript ID	LC-ART-12-2023-001044.R1
Article Type:	Paper
Date Submitted by the Author:	24-Jan-2024
Complete List of Authors:	Luan, Qiyue; University of Illinois at Chicago, Biomedical Engineering Pulido, Ines; University of Illinois at Chicago College of Medicine, Surgery Isagirre, Angelique; University of Illinois at Chicago, Biomedical Engineering Zhou, Jian; University of Illinois at Chicago, Biomedical Engineering Carretero, Julian; Universitat de València, Departament de Fisiologia, Facultat de Farmacia Shimamura, Takeshi; University of Illinois at Chicago College of Medicine, Surgery Papautsky, Ian; University of Illinois at Chicago, Biomedical Engineering

SCHOLARONE™
Manuscripts

Deciphering Fibroblast-Induced Drug Resistance in Non-Small Cell Lung Carcinoma through Patient-Derived Organoids in Agarose Microwells

Qiyue Luan,¹ Ines Pulido,^{2,3} Angelique Isagirre,¹ Julian Carretero,⁴ Jian Zhou,^{1,3} Takeshi Shimamura,^{2,3} and Ian Papautsky^{1,3*}

¹Department of Biomedical Engineering, University of Illinois Chicago, Chicago, IL 60607, USA

²Department of Surgery, University of Illinois Chicago, Chicago, IL 60612, USA

³University of Illinois Cancer Center, Chicago, IL 60612, USA

⁴Departament de Fisiologia, Facultat de Farmacia, Universitat de Valencia, Burjassot, 46010, Spain

*Address of correspondence

Dr. Ian Papautsky

Department of Biomedical Engineering

851 S. Morgan Street, 218 SEO

University of Illinois Chicago

Chicago, IL 60607, USA

E-mail: papauts@uic.edu; Tel: +1 312.413.3800

Abstract

Patient-derived organoids (PDOs) serve as invaluable 3D tumor models, retaining the histological complexity and genetic heterogeneity found in primary tumors. However, the limitation of small sample volumes and the lack of tailored platforms have hindered the research using PDOs. Within the tumor microenvironment, cancer-associated fibroblasts play a pivotal role in influencing drug sensitivity. In this study, we introduce an agarose microwell platform designed for PDO-based tumor and tumor microenvironment models, enabling rapid drug screening and resistance studies with small sample volumes. These microwells, constructed using 3D printing molds, feature a U-shaped bottom and 200 μm diameter. We successfully generated co-culture spheroids of non-small cell lung carcinoma (NSCLC) cells, including NCI-H358 or A549, and NSCLC PDOs F231 or F671 with fibroblast cell line, WI-38. Our results demonstrate the production of uniformly-sized spheroids (coefficient of variation <30%), high viability (>80% after 1-week), and fibroblast-induced drug resistance. The PDOs maintained their viability (>81% after 2-weeks) and continued to proliferate. Notably, when exposed to adagrasib, a KRAS^{G12C} inhibitor, we observed reduced cytotoxicity in KRAS^{G12C}-mutant spheroids when co-cultured with fibroblasts or their supernatant. The fibroblast supernatant sustained proliferative signals in tumor models. Taking into account the physical features, viability, and drug resistance acquired through supernatants from the fibroblasts, our platform emerges as a suitable platform for *in-vitro* tumor modeling and the evaluation of drug efficacy using patient-derived tissues.

Keywords

NSCLC, patient-derived organoid, co-culture, drug resistance, agarose microwells

1. Introduction

Lung cancer is the most common type of cancer worldwide, accounting for nearly 12% of all cancers [1, 2]. Non-small cell lung carcinoma (NSCLC), which accounts for 85% of all lung cancer diagnoses, has an overall 5-year survival rate of less than 26% in the United States [3]. Targeted therapies that focus on specific mutations or oncogenic rearrangements in cancer cells (e.g., EGFR, ALK, KRAS, MET, ROS1) [4] have shown to improve survival rates in NSCLC patients with these mutations [5]. However, the emergence of acquired mutations and drug resistance induced by the tumor microenvironment has led to attenuation in therapeutic efficacy.

The tumor microenvironment, which includes fibroblasts, malignant cells, endothelial cells, and immune cells, has a significant influence on cancer biology [6]. Cancer-associated fibroblasts (CAFs) in the tumor microenvironment have a secretory phenotype, releasing growth factors, cytokines, and chemokines into the extracellular matrix, that can directly or indirectly regulate tumor growth, survival, and drug response [7]. For example, the growth factors secreted by CAFs, such as hepatocyte growth factor (HGF), fibroblast growth factor (FGF), and insulin-like growth factor (IGF), can stimulate tumor proliferative capacity and resistance to anti-apoptotic stimuli [8]. The promotion of cancer cell proliferation is associated with drug resistance [9], resulting in therapeutic resistance of tumors that involve fibroblasts in the tumor microenvironment and negatively impact patient survival. Thus, drug screening using patient-derived materials should ideally incorporate tumor microenvironment components to better predict drug responses in patients.

A significant challenge in studying CAF-induced drug resistance is the scarcity of reliable preclinical models. Patient-derived organoids (PDOs) have gained widespread acceptance as an ideal 3D tumor platform to evaluating patient-specific drug response as they

retain the original tumor genotype and phenotype [10]. However, the doubling time of PDOs obtained from cancer patient biopsies tends to be slow [11] compared with the cells in 2D cultures [11, 12]. This discrepancy in growth rates poses limitations on PDOs' use in drug screening with conventional 96 to 384 well plates. Consequently, there is a pressing need for a high-throughput drug screening platform that requires only a small number of PDO cells. Furthermore, since CAFs have been shown to promote tumor growth and contribute to drug resistance, co-culturing them with PDOs can provide valuable insights into how to reconstruct tumor microenvironment *in vitro*, which will aid in the development of a more sophisticated screening platform that accounts for the influence of tumor microenvironment on the effectiveness of pharmacological agents.

Co-culturing PDOs and CAFs can be accomplished through either juxtacrine (contact-based) or paracrine (non-contact-based) co-culture methods [13]. In the former approach, both cell types are combined at a desired ratio and embedded in an extracellular matrix (ECM), such as Matrigel or collagen gel, to support cells in a complex 3D architecture that closely mimics the original tumor microenvironment [6], [14], [15], [16]. This method offers the advantage of precise control of over heterotypic and homotypic interactions, allowing for both physical contact and interactions through soluble factors. On the other hand, paracrine co-culture methods involve using membrane inserts to physically separate the co-cultured cells, enabling the study of cell signaling interactions between fibroblasts and tumor cells [17], [18], [19], [20]. This approach allows for the investigation of how each cell type responds individually, although it cannot completely prevent physical contact in the long term. It is important to note that both juxtacrine and paracrine co-culture methods necessitate the presence of fibroblast cells and come

with certain limitations, particularly in terms of the complexity of the culture when studying drug responses.

Microfluidic platforms offer a precise means to control the positioning of cells for juxtacrine and paracrine co-culture, facilitating the study of cell interactions and microenvironment conditions. This level of control is critical for research into cell behavior and tissue development *in vitro*. Different cell types can be strategically placed in defined patterns, separated by collagen [21], [22], membrane structures [23], or microcolumns [24], or they can be mixed within microfluidic devices to investigate cellular crosstalk and drug responses. Jang, et.al [21] applied collagen and micropost structure to separate pancreatic tumor spheroids, CAFs, and macrophage for paracrine co-culture. The collagen matrix between culture channels allowed cell-cell interaction for achieving activation and differentiation naive cells, promotion of EMT, and increasing of cancer cell invasion and migration. Emulate Inc.[25] applied membrane structure to separate upper ‘parenchymal’ channels for primary human hepatocytes, and lower ‘vascular’ channel for primary human liver sinusoidal endothelial cells, Kupffer cells, and stellate cells to build liver-on-chip. Based on this microfluidic platform, the co-culture liver model could replicate key histological structures and functions of the liver, and distinguish small-molecule toxic drugs and their non-toxic structural analogs. Ma, et.al. [24] used microcolumns to connect three culture chambers to study paracrine signaling between fibroblasts and cancer cell lines, as well as migration and trans-differentiation of fibroblasts. Thus, microfluidic technologies offer the ability to co-culture multiple cell types, facilitating studies on cell interactions.

While the co-culture of multiple cell types within microfluidic devices is feasible, this often necessitates intricate microfabrication processes and complex cell culture methods. This renders microfluidic co-culture a time-consuming and challenging undertaking. Furthermore, in

scenarios involving disease where only minimal tissue samples are available post-biopsy and where drug resistance inevitably arises, as observed in lung cancer, the utility of straightforward methods with uncomplicated workflows becomes apparent. The agarose microwells platform described in this work aims to seamlessly integrate into the existing well-plate workflow, enabling co-culturing with fibroblasts either in direct contact or in close proximity. This approach facilitates the investigation of potential paracrine-induced resistance. The intricacies associated with the aforementioned sophisticated microfluidic systems do not confer the desired advantages in this specific context. Thus, there is a critical need to develop a straightforward platform and culture method for co-cultivating PDOs and CAFs, streamlining the process and enhancing its accessibility.

In this study, we utilized an agarose microwells (AMWs) platform to facilitate the 3D culture of a tumor model with fibroblast cells or fibroblast supernatant. The primary objectives were to simplify co-culture procedure and investigate how fibroblasts promote drug resistance in NSCLC. Building upon our previous work [26], where we introduced a 3D culture platform based on AMWs for spheroid formation and *in vitro* cultivation of PDOs using minimal sample volumes, we extended the model by incorporating fibroblasts and fibroblast supernatant. The AMWs platform exhibits a smooth surface that allowed the migration of single cells or PDOs into the microwells within a day. Importantly, it maintained the viability and health of these cells over a two-week culture period. A single Matrigel dome provides sufficient PDOs to populate four wells in a 24-well plate. Our earlier work had successfully employed the AMW platform for targeted drug screening of EGFR-mutant NSCLC using EGFR tyrosine kinase inhibitors. The NSCLC cell line spheroids (A549, HCC4006, and NCI-H1975) successfully maintained >79% viability over 4-weeks in the AMW platform and showed the targeted drug response consistent

with the standard 2D-culture. In this study, we enhance the functionality of our platform to facilitate culture of primary tissue samples, incorporating co-culture with fibroblasts and fibroblast supernatant to replicate drug resistance induced by the tumor microenvironment. This enhancements aims to improve the efficacy of our NSCLC drug screening model. Additionally, this study transitions the agarose microwells to the higher throughput 48-well plate culture. We used genotyped NSCLC cell lines and PDOs with known sensitivity or resistance to targeted agents based on their KRAS^{G12C} genotype. We assessed the response of the tumor model with CAF-induced resistance to the FDA-approved therapeutic adagrasib (KRAS^{G12C} inhibitor). Our findings revealed that fibroblast supernatant significantly increased the viability of KRAS^{G12C} mutant cells under treatment, providing insights into how CAFs contribute to drug resistance. In summary, our platform offers a straightforward and cost-effective method for culturing PDOs to study drug response using fibroblast-conditioned medium to simulate the effects of the tumor microenvironment.

2. Results and discussion

2.1. Co-culture of NSCLC spheroids with fibroblasts in agarose microwells

Controlling the size of spheroids is critical because it significantly influences the physiological response of cells to the therapeutic compounds [25, 26]. Ensuring spheroid uniformity also yields results with low variation. Our agarose microwell platform proved effective in forming spheroids of uniform and predictable size. This was achieved by establishing a relationship between the initial seeding density and the resulting spheroid diameter [26]. Specifically, NCI-H358 and A549 were seeded at the density of 50 cells/microwells to form the spheroids with 80-100 μm diameters, closely resembling the $\sim 100 \mu\text{m}$ initial diameter of F231

and F671 PDOs. Fig. S1 shows images of spheroid arrays of co-culturing NSCLC cell lines and fibroblast WI-38 under various culture conditions, including NSCLC spheroids cultured in normal medium, NSCLC spheroids in WI-38 supernatant, and NSCLC mixed with WI-38 at different ratios to simulate the tumor microenvironment with varying fibroblast proportions. As evident in these images, cell aggregates formed in all co-culture conditions after 2 d of incubation, and tight spheroids were established after 4 d. Importantly, these spheroids exhibited reproducible sizes and shapes that enlarged based on the increasing fibroblast content. The coefficient of variation (CV) for the size of NCI-H358 spheroids cultured under normal medium, WI-38 supernatant, and mixed with WI-38 at ratios of 4:1, 1:1, and 1:4 were found to be 19%, 21%, 14%, 16%, and 22%, respectively. Similarly, the CVs of A549 spheroid size cultured under these respective conditions were 11%, 15%, 13%, 10%, 26% (Fig. 1A). These CV values consistent with the range reported in our previous work for HCC4006, NCI-H1975, and A549 spheroids (10%, 11%, and 22% respectively), and are notably lower than measurements obtained using low attachment plates (68%, 75%, and 80% respectively) [26] and dome PDOs culture (126.38%, $n=3$). These results underscore the capability of our agarose microwell platform to maintain predictable, uniform, and reproducible size in co-cultured NSCLC spheroids.

The biocompatible nature of agarose played a pivotal role in maintaining high cell viability on agarose microwells. Live/dead staining of spheroids cultured under different conditions on day 7 (Fig. 1B) revealed high viability (>80%), suggesting healthy cell culture conditions during the spheroid formation phase (2 d) and subsequent treatment (3 d). The viability of NCI-H358 spheroids cultured under normal medium, WI-38 supernatant, and mixed with WI-38 at ratios of 4:1, 1:1, and 1:4 were $91.0\pm 4.2\%$, $95.4\pm 3.2\%$, $89.1\pm 5.0\%$, $81.3\pm 6.3\%$, and $79.6\pm 6.0\%$, respectively. Similarly, the viability of A549 spheroids under these respective

conditions were found to be $99.8\pm 0.8\%$, $99.5\pm 1.4\%$, $98.6\pm 1.4\%$, $98.1\pm 1.7\%$, $99.0\pm 3.0\%$ (Fig. 1C). These consistently high viability rates serve as a strong foundation for ensuring the reliability and accuracy of drug screening results.

2.2. Evaluating drug response on NSCLC and fibroblast co-cultured spheroids

Targeted drug therapy is expected to induce a cytotoxic effect, leading to apoptosis in cells within spheroids [29]. In this study, we used adagrasib (MRTX849), a small molecule covalent inhibitor of KRAS^{G12C} FDA-approved for the use in patients with locally advanced or metastatic NSCLC harboring KRAS^{G12C} [30]. In Fig. 2A, representative images illustrate the cell viability of NCI-H358/A549 co-cultured spheroids with WI-38 fibroblasts following exposure to various concentrations of adagrasib. Consistent with findings in 2D cultures, we observed that NCI-H358 spheroids, which harbor the KRAS^{G12C} mutation, were sensitive to adagrasib in dose-dependent manner. In contrast, A549 spheroids, which harbors KRAS^{G12S} mutation, showed no response to adagrasib. Interestingly, both co-culturing with WI-38 and WI-38 supernatant promoted drug resistance in NCI-H358 cells to adagrasib. This observation suggests that fibroblasts and fibroblast supernatant play a role in alleviating cytotoxic effects of the drug on target cells.

To assess the impact of fibroblasts and fibroblast supernatant on drug resistance, we conducted a comparative analysis of spheroid viability and sizes after a 72h-exposure to adagrasib. NCI-H358 spheroids cultured in standard medium exhibited remarkable sensitivity to adagrasib, with ~64% of cells experiencing cell death following exposure to an adagrasib concentration of 250 nM. When these spheroids were cultured in WI-38 supernatant under the same drug concentration, only ~10% of cells underwent apoptosis (Fig. 2B). In addition, WI-38

supernatant contributed to the maintenance of spheroid size under the treatment conditions (Fig. 2C). These findings indicate a significant drug-resistant effect of fibroblast supernatant ($p < 0.001$, $n = 56$). Spheroids composed of A549 cells lacking the KRAS^{G12C} mutation did not respond to adagrasib treatment, evident in both viability and spheroid size outcomes (Fig. 2D and Fig. 2E, respectively).

While NCI-H358 spheroids co-cultured with WI-38 cells exhibited reduced cell death in a manner dependent on the amount of WI-38 cells present, it is important to note that the result is the sum of viability of both NCI-H358 and WI-38 cells. Even when accounting for the presence of adagrasib resistant WI-38 cells, the cytotoxic impact of adagrasib on co-cultured spheroids proved to be more pronounced than that observed in NCI-H358 spheroids cultured in WI-38 supernatant alone. These findings strongly suggest that factors in fibroblast supernatant significantly enhance drug resistance in NCI-H358 spheroids. Furthermore, after a 72h-exposure to 500 nM adagrasib, the size of spheroids cultured in WI-38 supernatant reduced to 48% of their original size, while spheroids in the standard culture medium shrank to 27% of their initial size. This suggests that spheroid size was better preserved in fibroblast supernatant during the treatment. These results align with the cytotoxicity assessment described earlier, further reinforcing the idea that spheroids cultured in fibroblast supernatant exhibit heightened drug tolerance, as evidenced by consistently lower rates of cell death.

2.3. Culture of PDOs in agarose microwells

To illustrate the capability of our agarose microwell platform in supporting *in vitro* cultivation of patient-derived tissues, we used two types of NSCLC PDOs, namely F231 and F671. These PDOs harboring KRAS^{G12C} mutation were sourced from the National Cancer

Institute (NCI) Patient-Derived Models Repository (PDMR). PDOs represent a valuable model for cancer research as they closely replicating the histopathology, gene expression profile, and treatment sensitivity of the primary tumors [31]. This renders cancer PDOs an invaluable tool for implementing personalized medicine approaches aimed at predicting the effectiveness of anti-cancer treatments *ex vivo*. In our study, we cultured and treated these PDOs using our agarose microwell platform. This study served both as a proof-of-concept, demonstrating the compatibility of our platform with PDOs and as an extension of our earlier investigation into drug response of KRAS^{G12C} inhibitor using the NCI-H358 cell line model.

NSCLC PDOs, F231 and F671, were cultured for 3 weeks in our agarose microwell platform. To evaluate the viability and health of these PDOs, we performed live/dead staining on days 2, 7, 14, and 21. The viability of F231 PDOs remained consistently high throughout the culture period (Fig. 3A). Specifically, the viability was recorded as $98.8 \pm 3.8\%$ on day 2, $89.5 \pm 7.1\%$ on day 7, $81.5 \pm 6.7\%$ on day 14, and $77.9 \pm 8.6\%$ on day 21 ($n = 20$). Similarly, F671 PDOs demonstrated high viability over the three-week culture, with recorded viabilities of $90.7 \pm 9.3\%$ on day 2, $92.0 \pm 6.0\%$ on day 7, $85.7 \pm 7.4\%$ on day 14, and $81.0 \pm 7.1\%$ on day 21 ($n = 20$) (Fig. 3B). In comparison to the conventional approach of embedding PDOs in BME2 (basement membrane extract type 2), our agarose microwell platform demonstrated a significant advantage in sustaining long-term studies involving patient-derived samples, while maintaining consistently high viabilities. Typically, PDOs cultured using the BME2 embedding method exhibited viabilities ranging from 61% to 79% after one month of incubation [32]. For further comparison, we cultured F231 PDO in Matrigel dome and showed high viability ($91.4 \pm 11.6\%$) after 7 d, which is consistent with the PDOs cultured in our AMWs. Nevertheless, as Fig. 3D illustrates, a significantly greater variance in size was observed for PDOs in Matrigel dome after

7 d ($CV = 126.4 \pm 40.1\%$, $n=3$) in comparison to the notably smaller variations observed in AMWs ($CV = 15.4\%$ for F231 and $CV = 18.8\%$ for F671). The consistently high viabilities observed in our platform affirm its suitability for long-term culture and studies with patient-derived samples.

Following a week of incubation in agarose microwells, we observed that PDOs maintained viabilities exceeding 90%, indicating stable and healthy cell conditions throughout the drug screening process. However, as the incubation period extended beyond two weeks, a slight decrease in viability occurred, transitioning from >90% to >77% between days 14 and 21. This gradual decline in viability with time can be attributed to several factors, including the enlargement of PDOs leading to spatial differences, limitations in nutrient availability, suboptimal oxygen level, and the accumulation of metabolic waste in the wells [33]. Additionally, the inability to passage the PDOs during three-week incubation period contributed to the accumulation of dead cells. It is worth noting that the gradual decline of PDO viability beyond two weeks is in line with results obtained using the standard Matrigel dome culture method [32]. However, it is important to highlight that in our agarose microarray, PDOs consistently maintained high viability (>90%) throughout the entire duration of drug treatment. This demonstrates that the platform's compatibility with patient-derived samples and its capacity to facilitate patient-specific drug screening applications in real time.

Simultaneously with our viability assessments, we analyzed PDO growth over a 3-week period (Fig. 3C). During the initial two weeks, both F231 and F671 PDOs displayed growth trends, with F231 expanding from approximately $28000 \mu\text{m}^2$ to $41000 \mu\text{m}^2$ and F671 increasing from roughly $25000 \mu\text{m}^2$ to $60000 \mu\text{m}^2$. This phase of exponential growth aligns with observations made in the standard BME2 dome 3D-culture method, where spheroid size

increased steadily without disaggregation between day 3 to day 15 [34]. However, as we extended the incubation period into the 3rd week in our agarose microwells, a reduction in size was observed. Specifically, F231 PDOs decreased from approximately 41000 μm^2 to 37500 μm^2 , while F671 PDOs decreased from $\sim 60000 \mu\text{m}^2$ to $\sim 57000 \mu\text{m}^2$. Notably, these modest reductions in size during the latter part of the three-week duration corresponded with a slight decrement in the viability of the PDOs.

2.4. Assessment of drug response of PDOs cultured with fibroblast supernatant

We conducted a comparative analysis of the impact of fibroblast supernatant on PDO drug sensitivity, extending our examination to the cell line spheroid models. Building on our previous findings, we co-cultured KRAS^{G12C}-mutant PDOs, F671 and F231, with fibroblast supernatant in agarose microwells and assessed cytotoxicity. These PDOs were grown under normal culture medium, WI-38 supernatant, and CAF supernatant in agarose microwells and subsequently treated with adagrasib. Images in Fig. 4A clearly illustrate that both F231 and F671 PDOs are sensitive to adagrasib. However, when cultured with WI-38 and CAF supernatants, the cytotoxic effect was mitigated, as illustrated by reduced red signal indicative of decreased cell death and preservation of PDO size. This observation aligns with the outcomes observed in NCI-H358 spheroid models, highlighting the consistent effect of fibroblast supernatant on PDOs drug sensitivity.

To quantitatively assess the drug-resistant effect of WI-38 and CAF supernatant on KRAS^{G12C}-mutant PDOs, we compared viabilities of PDOs cultured with normal medium and fibroblast supernatant (Fig. 4B). Both F671 and F231, which are inherently sensitive to adagrasib due to the KRAS^{G12C} mutation, the introduction of WI-38 and CAF supernatant increased

viabilities. Specifically, for F671 viabilities rose from $69.6 \pm 16.9\%$ to $80.2 \pm 9.0\%$ ($p < 0.0001$, $n_{\text{normal medium}}=97$, $n_{\text{WI-38 supernatant}}=41$) and $87.8 \pm 5.6\%$ ($p < 0.0001$, $n_{\text{CAF supernatant}}=44$), respectively, following 72 h treatment of 500 nM adagrasib. For F231, viabilities increased from $45.3 \pm 21.3\%$ to $60.6 \pm 9.6\%$ ($p < 0.001$, $n_{\text{normal medium}}=61$, $n_{\text{WI-38 supernatant}}=32$) and $71.1 \pm 20.9\%$ ($p < 0.0001$, $n_{\text{CAF supernatant}}=55$), respectively, for the same treatment conditions. These results underscore the significant role of fibroblast supernatant in reducing cell death and sustaining cell proliferation during targeted anti-cancer treatment. Also, compared with other co-culture methods using fibroblast cells [35], using fibroblast supernatant simplified the operation complexity, while also simulate the fibroblast-induced drug resistance.

2.5. Growth factors secreted by fibroblasts promote drug resistance

Drug sensitivity can be influenced by several factors that maintain proliferative signals active within the TME [36]. These signaling pathways lead to increased tumor proliferation, ultimately contributing to resistance against cancer therapies [37]. Thus, understanding the biological mechanisms underlying the fibroblast supernatant-induced resistance can be crucial for developing models that incorporate both tumor and microenvironment factors to evaluate drug sensitivity and overcome fibroblast-induced resistance. To investigate whether the maintenance of proliferative signals requires fibroblast cells or just fibroblast supernatant, we co-cultured NCI-H358 with WI-38 cells (NCI-H358: WI-38 \approx 1:5) in agarose microwells. We also cultured NCI-H358 with WI-38 supernatant harvested from the same number of WI-38 cells. We compared the cytotoxic effect of adagrasib on these cultures. Results in Fig. 5A reveal that, compared with NCI-H358 spheroids cultured in normal medium, both NCI-H358 spheroids with added WI-38 supernatant and NCI-H358+WI-38 spheroids exhibited significantly increased viability under 250 nM adagrasib ($p < 0.0001$, $n=36$) and 500 nM adagrasib ($p < 0.0001$, $n=36$).

This finding suggests that drug resistance can be induced by both WI-38 cells and WI-38 supernatant, implying that fibroblasts secrete growth factors capable of enhancing drug resistance.

Although in NCI-H358+WI-38 mixture spheroids, the cell number of WI-38 with WT-KRAS was 5× greater than the number of NCI-H358 cells, the viability of these co-cultured spheroids only slightly exceeded that of NCI-H358 spheroids in WI-38 supernatant by 10.6% and 15.1% following 250 nM and 500 nM adagrasib treatments, respectively. Thus, it appears that secretory factors from fibroblasts in the supernatant are the dominant factor responsible for the drug resistance induction. The role of direct cell-cell interactions in this process appears to be relatively minor. Consequently, fibroblast supernatant can be used for studying drug resistance in tumors.

To further investigate if the factors secreted by fibroblasts into the culture media contribute to drug resistance, we conducted a cytotoxicity experiment using serial dilutions of WI-38 supernatant. NCI-H358 spheroids were treated with WI-38 supernatant diluted 0, 1, 2, 3 times in addition to normal culture medium. As the WI-38 supernatant became more diluted, the viability of NCI-H358 spheroids following treatment decreased and approached the cytotoxicity observed in the normal culture medium group (Fig. 5B). These findings strongly suggest that the secreted factors present in WI-38 supernatant indeed play a significant role in promoting drug resistance, and the concentration of these secreted factors is a critical factor influencing drug resistance.

In addition to conducting cytotoxicity assessments, we undertook an investigation into the active state of surviving spheroids by immunofluorescent staining the proliferation biomarker Ki67 in NCI-H358 spheroids, after their exposure to fibroblast supernatant and standard culture

medium (Fig. 6A). For the purpose of quantifying Ki67 expression levels in NCI-H358 spheroids following 48h of adagrasib treatment administered with conventional culture medium and WI-38 supernatant, we employed the Ki67/Hoechst area ratio (Fig. 6B). The outcomes of our analysis showed the elevated Ki67/Hoechst ratio in the WI-38 supernatant-exposed group in comparison to the normal medium-treated group, thereby affirming the substantive contribution of supernatant constituents to the sustenance of proliferative capabilities in NCI-H358 spheroids during the drug treatments. Specifically, the WI-38 supernatant led to a conspicuous augmentation in the Ki67/Hoechst ratios of NCI-H358 spheroids, transitioning from $68.3 \pm 25.4\%$ to $98.1 \pm 5.3\%$ ($p < 0.001$, $n=12$) and from $74.1 \pm 19.6\%$ to $84.9 \pm 19.7\%$ ($p < 0.05$, $n=23$) subsequent to adagrasib treatment at concentrations of 250 nM and 500 nM, respectively. This observed enhancement in Ki67 expression underscores the ability of molecules secreted by fibroblasts to uphold the proliferative potential of cancer cells even in the presence of tyrosine kinase inhibitors, thereby underscoring the imperative of evaluating cell cytotoxicity within the broader context of interactions with other tumor-associated cellular components.

We extended our evaluation to understand the impact of fibroblast supernatant on the maintenance of proliferative signals. We investigated the effect of supernatant from immortalized WI-38 fibroblasts as well as patient-derived NSCLC fibroblasts: CAF41 (derived from EGFR^{mut} patient) and CAF63 (obtained from a KRAS^{mut} patient). Interestingly, we used fibroblasts derived from tumors with different genetic backgrounds to assess potential genetic-specific effects. Our findings revealed that all three different fibroblast supernatant samples could help sustain the phosphorylation of ERK, a surrogate marker for proliferation, albeit at varying levels (Fig. 7A). Importantly, this correlated with higher levels of ATP after adagrasib treatment (Fig. 7B). These results suggest that various fibroblast sources can contribute to

maintaining proliferative signals in cancer cells, highlighting the significance of understanding the diverse influences of the CAFs on drug responses.

Given that the modulation of drug resistance appears to be dependent on the secreted factors of each fibroblast, we evaluated the specific growth factors present in their supernatants (Fig. 7C-D). As expected, each fibroblast type secreted a distinct set of growth factors. Interestingly, CAF63 supernatant contained a higher overall amount of growth factors compared with the other samples, even though its effect on drug resistance was relatively smaller. This led us to hypothesize that the growth factors found in higher concentrations in both WI-38 and CAF41 supernatants, and to a lesser extent in CAF63 supernatant, might be the key players in promoting drug resistance in NSCLC harboring KRAS^{G12C}. Among these growth factors, HGF was noteworthy as it was secreted by all three fibroblast types but more abundantly by WI-38 and CAF41, and less so by CAF63, which correlated with the results of the cell cytotoxicity assays. To further investigate this, we used the FDA-approved MET inhibitor cabozantinib to assess whether pharmacological inhibition of secreted HGF could re-sensitize NCI-H358 cells to adagrasib. As observed previously, NCI-H358 cells cultured with WI-38 supernatant and challenged with adagrasib could sustain pERK proliferation signals. However, MET inhibition counteracted this effect (Fig. 7E), effectively re-sensitizing cells to G12C inhibitors (Fig. 7F). These findings underscore the potential of targeting specific growth factors, like HGF, to overcome fibroblast-induced drug resistance in cancer therapy.

3. Conclusions

This work describes a successful application of an agarose microwell platform for studying drug resistance in PDOs. The platform offers several advantages, including consistent

spheroid size, high spheroid viability, and the ability to maintain PDO health for 2 weeks. These features make it suitable for conducting co-culture experiments and drug screening, with the added benefits of requiring smaller sample sizes and shorter incubation times compared to standard PDO culture methods. One significant finding of this work was the successful induction of drug resistance in PDOs using fibroblast supernatants, this represents a simplified approach compared to co-culturing with fibroblast cells. In this method, only the conditioned culture media from fibroblast supernatants are used, yet it effectively maintained signals that promote drug resistance in PDOs harboring KRAS^{G12C}. The concentration of growth factors, such as HGF, in these supernatants is found to correlate with increased proliferation and resistance to adagrasib. Further investigations using western blot and immunostaining demonstrate elevated expression of proliferation biomarkers in PDOs cultured in fibroblast supernatants compared to those cultured in normal culture medium.

Additionally, this study describes an innovative platform for investigating drug resistance in PDOs and demonstrates a simplified alternative method to co-culturing multiple cell types within microfluidic devices. The use of microfluidic platforms in modeling tumors and their microenvironments has become increasingly popular due to their ability to replicate multicellular architecture and physicochemical conditions. Various cell types, including cancer cells, fibroblasts, immune cells, and endothelial cells, have been incorporated into various microfluidic co-culture platforms, [38], [39] successfully demonstrating cancer phenotype modelling and drug response results. However, these systems often demand complex co-culturing techniques, presenting a potential challenge. The findings presented here suggest a promising alternative approach by employing conditioned media from various cell types, including fibroblast supernatants, as a substitute for direct cell-cell co-cultures. This streamlines the experimental

process and enhances the feasibility of employing microfluidic devices for tumor modeling and related research.

Similar microwell array structures have been used in other microfluidic devices for PDO culture [40], [41]. Choi, et al.[41] designed a microfluidic device using microwells for on-chip culture of pancreatic cancer PDOs, demonstrating successful outcomes in drug screening for chemotherapy and immunotherapy. However, the limit of a one-week on-chip culture duration and the requirement to seed only single cells, followed by a subsequent formation process, impose time constraints on the of drug treatment studies. In contrast, our AMW platform exhibits the capacity to culture single cells, form spheroids, and enable arrangement of PDO fragments for drug screening within a single day of pre-treatment culture. Liu, et. al.[40] developed an array of microwells with a 1 mm diameter, 200 μm depth, and a 1.25 mm pitch for the freeze-thaw procedure of PDOs, on-chip culture, and drug sensitivity testing. Nevertheless, in comparison to our AMW platform, the larger size of the microwells and the presence of multiple PDOs in each well lead to significant size variability. It is reported that variations in spheroid size may yield different drug responses [28], potentially impacting the outcomes of drug testing. The use of AMW to achieve smaller size variability could contribute to more consistent drug response outcomes. In summary, our work presents a significant advancement in the field of precision medicine and tumor modeling. The use of fibroblast supernatants to replicate the tumor microenvironment simplifies co-culturing procedures and expands the potential of microfluidic devices for applications related to drug resistance and precision medicine applications.

4. Materials and Methods

4.1. Materials

Cell lines (A549, NCI-H358, and WI-38) were purchased from ATCC (Manassas, VA, USA) and maintained as specified. F231 and F671 NSCLC PDOs were obtained from NCI patient-derived models repository (PDMR). RPMI 1640 medium with L-glutamine, EMEM medium, DMEM medium, trypsin–EDTA (0.25%), 1× phosphate buffered saline (PBS), Dispase II, and 24/48-well cell culture plates were purchased from Fisher Scientific (Waltham, MA, USA). Fetal bovine serum (FBS) was purchased from GeminiBio Inc. (West Sacramento, CA, USA). 100× antibiotic–antimycotic, calcein AM viability dye, Bis-Tris Plus Mini Protein Gels, 4–12% were purchased from Invitrogen (Carlsbad, CA, USA). Agarose powder was purchased from Sigma-Aldrich (St. Louis, MO, USA). Propidium iodide was purchased from Alfa Aesar (Haverhill, MA, USA). Hoechst 33342 Solution was purchased from Thermo Fisher Scientific (Heretofore TFS, Waltham, MA, USA). Adagrasib was purchased from MedChemExpress (Monmouth Junction, NJ, USA). CellTiter-Glo® 3D Cell Viability Assay was purchased from Promega (Madison, WI, USA). Mouse anti-Ki67 antibody, goat anti-rabbit IgG H&L (Alexa Fluor® 647), 10×blocking reagent, and Growth Factor Human Membrane Antibody Array were purchased from Abcam (Waltham, MA, USA). Basement Membrane Extract Type 2 (BME2) was purchased from R & D Systems (Minneapolis, MN, USA).

4.2. STR assay

Cell line authentication was confirmed by STR analysis. DNA was extracted using the DNeasy Blood and Tissue Kit (Qiagen) and DNA samples were quantified using NanoDrop ND-2000 (Thermo Fisher Scientific) to ensure quality. Samples were submitted to the Genomic Research-DNA services Facility at Northwestern University for STR profiling. Results (Table S1) were compared to known STR profiles for NSCLC cell lines available on the ATCC website.

4.3 NSCLC cell lines and PDOs culture conditions

Prior to seeding cells into agarose microwells, NSCLC cell lines A549/NCI-H358 and fibroblast cell line WI-38 were incubated in RPMI 1640 medium and EMEM medium respectively supplemented with 10% (v/v) FBS, and 1% (v/v) 100× antibiotic–antimycotic solution. Cells were maintained at 37 °C and 5% CO₂.

PDOs F231 and F671 were obtained from the NCI PDMR repository and maintained as specified. PDOs were grown in complete media 6A (50% L-WRN conditioned media, 1.25mM L-acetylcysteine, 10mM nicotinamide, 1X N21 MAX Media Supplement, 1X N-2 MAX Media Supplement and 10 μM Y-27632). Organoids were grown in BME2 domes until confluency was reached. Then, domes were disaggregated with Dispase II for 2h at 37°C, then organoids were collected and centrifuged 5 min at 200g prior seeding in agarose microwells for viability assays.

4.4. Establishment of patient-derived cancer-associated fibroblasts

Tumor biopsy samples were received from patients at Hospital Universitario de la Ribera (Alzira, Spain). All patients signed informed consent to participate in protocol approved by the Institutional Review Board giving permission for research to be performed on their samples. Patients resections were placed in a sterile tube containing complete DMEM media (10% FBS and 1% antibiotic-antimycotic) and transported on ice from the operating room to the research laboratory. Biopsies were minced with sterile scalpels and then enzymatically digested with Liberase TM (Roche) for 1 hour in agitation. After digestion, cells were seeded on dishes with complete DMEM (10% FBS). Fibroblasts were naturally selected as they competed out other cell types. The clinicopathologic features of the patients are listed in Table S2.

4.5. Agarose microwell fabrication and co-culture spheroids formation

The agarose microwells were 200 μm in diameter and 75 μm deep and made by casting on polydimethylsiloxane (PDMS) replicas of 3D-printed masters. The agarose microwell fabrication was based on the protocol reported in our previous publication [26]. The resulting constructions were \sim 400 agarose microwells molded per well of 24-well plates and \sim 150 agarose microwells molded per well of 48-well plates.

To achieve the target of co-culture cancer cells with fibroblasts, 1 mL of NCI-H358/A549 and WI-38 mixture suspensions were pipetted into wells of 24-well plate; each well of the plate contained an agarose insert with 400 microwells. In cell mixture suspension, the concentration of NCI-H358/A549 was 20000 cells per mL (\sim 50 cells per microwell) and concentrations of WI-38 were 5000, 20000, and 80000 cells per mL to achieve the cell number ratio of NCI-H358/A549: WI-38 of \sim 4:1, 1:1, 1:4. Mixing the cell suspension thoroughly before seeding cells in agarose wells to decrease variability of the cell number in each microwell. Seeded cell mixtures of NCI-H358/A549 and WI-38 were cultured in RPMI 1640 medium with L-glutamine supplemented with 10% (v/v) FBS, and 1% (v/v) antibiotic-antimycotic (100 \times). Besides the co-culture of NCI-H358/A549 with fibroblasts, we also seeded NCI-H358/A549 into WI-38 fibroblast supernatant at the same seeding density of 20000 cells per mL (\sim 50 cells per microwell). To keep the repeatability and enough fibroblast secretions harvested in the supernatant, the fibroblast supernatant was collected after 2 d of incubation of WI-38 with 100% confluence. After 2 d of incubation, the heterogeneous cell spheroid with NSCLC cells and fibroblasts and homogenous spheroids only containing NCI-H358 or A549 cells were all formed in each agarose microwell.

4.6. Spheroids phenotypes evaluations

For all homogenous spheroids and co-cultured mixture spheroids, spheroid viability was evaluated at day 7 after seeding. The staining solution was culture media supplemented with $3 \mu\text{g mL}^{-1}$ of live cell dye calcein AM (495/515 nm ex/em), $3 \mu\text{g mL}^{-1}$ of dead cell dye propidium iodide (PI) (535/617 nm ex/em), and $3 \mu\text{g mL}^{-1}$ of nuclear dye Hoechst 33342 (361/497 nm ex/em). Then, 1 mL of staining solution was added to wells of 24-well plate and incubated for 30 min at 37°C . Live/ dead images of spheroids were captured by the z-stack function with 5 planes using an Olympus IX-83 fluorescence microscope. Live/dead images were analyzed using Olympus CellSens software by comparing the total area of the calcein AM signal of all planes with the total area of the (calcein AM + PI) signals of all planes. This image-based viability measurement method was consistent with the standard 3D cell viability assessment method CellTiter-Glo® ATP luminescence assay (Fig. S2). The results were analyzed and plotted using Origin 2021 (OriginLab Corporation).

The spheroid size was evaluated based on spheroid cross-section area using calcein AM signal in live/dead fluorescent images captured above. We analyzed the plane in live cell z-stack images that focusing the largest cross section for spheroid size measurements. 56 spheroids of each culture condition were traced using Olympus CellSens software to estimate the average and standard deviation (STD) of spheroid cross-section area. The coefficient of variation (CV) of spheroid size was cultured by $\text{STD/average}\%$. Spheroid size results were analyzed and plotted using Origin 2021 (OriginLab Corporation).

4.7. PDOs culture in agarose microwells

300 μL of PDOs suspension containing ~ 150 PDOs were pipetted into wells of a 48-well plate; each well of the plate contained an agarose insert with 150 microwells. Mixing the PDO suspension thoroughly after seeding PDOs in agarose wells to separate the PDOs evenly into microwell arrays and formed PDO arrays after overnight incubation. For viability and size assessments, PDOs were evaluated at days 2, 7, 14, 21 after seeding. PDO viability and size evaluations followed the same protocol of spheroid live/dead staining and cross-section area measurement described above.

4.8. Drug exposure and drug response studies

NSCLC NCI-H358 and A549 homogenous spheroids and co-cultured mixture spheroids with fibroblasts residing in agarose microwells were firstly incubated under WI-38 supernatant and normal culture medium, respectively, for 2 d and then exposed to KRAS^{G12C} inhibitor adagrasib for another 3 d. The range of drug concentrations was 0 nM, 250 nM, 500 nM, 1 μM , and 2 μM . Drug response assessments including cytotoxicity evaluation and spheroid size measurement after treatments followed the same protocol of spheroid live/dead staining and cross-section area measurement described above. The assays were conducted in duplicate, and the average relative viability and average relative spheroid size were determined for each experimental condition. Spheroid relative viability was calculated as the percentage of treatment group spheroid viability relative to control group spheroid viability, while spheroid relative size was calculated as the spheroid size of the treatment group relative to the control group spheroid size for each respective condition. The results were analyzed and plotted using Origin 2021 (OriginLab Corporation).

F231 and F671 PDOs seeded in agarose microwells were firstly incubated under the normal culture medium for 1 d and then exposed to 500nM adagrasib with normal culture medium, WI-38 supernatant, and CAF supernatant for another 3 d. Drug response assessment - cytotoxicity evaluation followed the same protocol of spheroid live/dead staining described above. The comparisons between culture conditions considering two independent variables (adagrasib treatment and culture media) were analyzed by two-way ANOVA. The average relative viabilities and comparisons of all treatment conditions were plotted by GraphPad Prism 10.0.1 (GraphPad Software, Inc).

4.9. Comparing the contributions of fibroblast and fibroblast supernatant to drug resistance

The contributions of fibroblast cells and fibroblast supernatant to NCI-H358 drug resistance were compared by cytotoxicity assays on NCI-H358+WI-38 mixture spheroids and NCI-H358 spheroids under WI-38 supernatant. The WI-38 was cultured in 24-well plates at 100% confluence and its supernatant was maintained in plates for 2 d before being used in cytotoxicity assays to harvest enough fibroblast secretion. To make sure the WI-38 numbers that offered supernatant and mixed with NCI-H358 are the same, we collected the WI-38 supernatant and all WI-38 cells from the same well of 24-well plate and then mixed the collected supernatant and WI-38 cells with 20000 NCI-H358 cells separately before pipetted into each well of 24-well plate with agarose microwell insert. After spheroids formation, exposing the spheroids to 500 nM adagrasib for 3 d, and then the cytotoxicity evaluation was followed the same protocol described above.

In addition to the fibroblast cells and fibroblast supernatant comparison, the WI-38 supernatants with different dilution times were used to culture NCI-H358 spheroids to verify the

drug resistance effects of fibroblast secretion concentration. WI-38 supernatant was diluted by NCI-H358 culture medium at the dilution times of 0, 1, 2, 3, and then mixed with NCI-H358 cells in microwell arrays. The NCI-H358 spheroids formed under the WI-38 supernatant and were then treated with 500 nM adagrasib for 3 d. NCI-H358 spheroids formation and cytotoxicity evaluation followed the same protocols described above. The results were analyzed and plotted using Origin 2021 (OriginLab Corporation).

4.10. Mechanism studies of fibroblast supernatant-induced drug resistance

Cell proliferation in NCI-H358 spheroids cultured under WI-38 supernatant and normal medium was evaluated by immunofluorescently staining cell proliferation biomarker Ki67. After cultivation and 500 nM adagrasib treatment in agarose microwells, spheroids were washed with 1× PBS and fixed with 4% paraformaldehyde solution for 30 min at ice-cold temperature and then washed with 1× PBS. Subsequently, fixed spheroids were blocked with 1× blocking buffer for 1 h at room temperature for nonspecific binding. The spheroids were then incubated with 2.5 $\mu\text{g mL}^{-1}$ rabbit anti-Ki67 antibodies overnight at 4 °C. Then the spheroids were washed with 1×PBS 3 times and incubated with 2.5 $\mu\text{g mL}^{-1}$ goat anti-rabbit IgG H&L (Alexa Fluor® 647) overnight at 4 °C. Then the spheroids were washed with 1× PBS 3 times and incubated with 3 $\mu\text{g mL}^{-1}$ of nuclear dye Hoechst 33342 for 30 min. Then washing spheroids with 1× PBS 3 times before imaging to avoid background noise. Afterwards, stained cells were visualized and imaged using Olympus IX- 83 fluorescence microscope. The areas of Ki67 and Hoechst signals were analyzed by Olympus CellSens software. The difference between two culture conditions was analyzed by two-sample t-test.

In addition to the immunofluorescence staining, the western blot of proliferation biomarkers was used to further study the pathways of the drug resistance mechanism. Monolayer of NCI-H358 cultured in 6-well plates under the normal medium, WI-38 supernatant, and cancer-associated-fibroblast supernatant was treated by 0 nM and 500 nM adagrasib for 72 h. After seeding and drug treatments, cells were washed with cold PBS and lysed with CST lysis buffer plus phosphatase and protease inhibitors. Lysates were centrifuged at 4°C and quantified with BCA method (Pierce #23224). Samples were prepared with Novex buffers and 40 µg of lysates were loaded and run on Invitrogen 4-12% Bis-Tris gels followed by transfer to nitrocellulose membranes. Membranes were incubated overnight with the indicated primary antibodies and then washed and incubated with anti-rabbit secondary antibodies. Detection was performed using an iBright 1500 (ThermoFisher).

Along with the western blot assay, the same batch of NCI-H358 cells used for western blot was mixed with the same batch of fibroblast supernatants and normal culture medium respectively and seeded 300 µL cell suspension into the well of 48-well plate with agarose microwell insert at the seeding density of 25000 cells per mL (50 cells per microwells). NCI-H358 cells residing in agarose microwells were first incubated for 2 d to form spheroids and then exposed to 500 nM adagrasib for 24 h. The cytotoxicity was evaluated by ATP luminescent cell viability assay. Add 300 µL CellTiter-Glo 3D reagent into each well and mix the reagent with spheroid suspension by shaking for 5 min. The mixture of CellTiter-Glo 3D reagent and cell samples was incubated at room temperature for 30 min at dark, and then removed to a white 96-well plate. The luminescence intensity was recorded by Synergy LX multi-mode reader (BioTek).

A panel of 41 human growth factors was evaluated in cell-cultured media using the Growth Factor Human Membrane Antibody Array (abcam), according to the manufacturer's instructions. Membranes were imaged and signal densities for individual antigen-specific antibody spots between arrays were analyzed with HImage++ (Western Vision Software). Background was subtracted from the raw densitometry data and results were normalized to the reference signals. Growth factors relative expression was transformed in log₂ and data was plotted in Morpheus ("<https://software.broadinstitute.org/morpheus/>"Broad Institute).

Acknowledgements

Funding: This work was supported in part by the Departments of Biomedical Engineering and Surgery at the University of Illinois Chicago, NIH award R01CA230778, and DoD Concept Award (W81XWH2210023). **Author Contributions:** Q. Luan, I. Pulido, and A. Isagirre conducted the experiments; J. Zhou, T. Shimamura, and I. Papautsky conceived the idea and designed the experiments. Q. Luan, I. Pulido, J. Zhou, T. Shimamura, and I. Papautsky contributed equally to the writing of the manuscript. **Conflicts of Interest:** The authors declare no conflict of interest.

Data Availability

The data supporting this study are available from the corresponding author.

Supplementary Materials

Figure S1. NSCLC cell lines A549 and NCI-H358 were co-cultured with fibroblasts in agarose microwells and formed tight spheroids.

Figure S2. The comparison of 3D cell viability evaluation methods between live/dead staining images and ATP luminescence assays.

Table S1. STR profiles of the cell lines A549, NCI-H358, and WI-38 used in this study.

Table S2. The clinicopathological features of the patients from whom the CAF41/CAF63 were derived.

References

- [1] J. D. Minna, J. A. Roth, and A. F. Gazdar, “Focus on lung cancer,” *Cancer Cell*, vol. 1, no. 1, pp. 49–52, Feb. 2002, doi: 10.1016/S1535-6108(02)00027-2.
- [2] L. A. Torre, R. L. Siegel, and A. Jemal, “Lung Cancer Statistics,” in *Lung Cancer and Personalized Medicine: Current Knowledge and Therapies*, A. Ahmad and S. Gadgeel, Eds., in *Advances in Experimental Medicine and Biology.*, Cham: Springer International Publishing, 2016, pp. 1–19. doi: 10.1007/978-3-319-24223-1_1.
- [3] “Lung Cancer - Non-Small Cell - Statistics,” Cancer.Net. Accessed: Jan. 30, 2023. [Online]. Available: <https://www.cancer.net/cancer-types/lung-cancer-non-small-cell/statistics>
- [4] M. R. Waarts, A. J. Stonestrom, Y. C. Park, and R. L. Levine, “Targeting mutations in cancer.” Accessed: Jul. 01, 2023. [Online]. Available: <https://www.jci.org/articles/view/154943/table/1>
- [5] D. E. Gerber, “Targeted Therapies: A New Generation of Cancer Treatments,” *Target. Ther.*, vol. 77, no. 3, 2008.
- [6] S. Tsai *et al.*, “Development of primary human pancreatic cancer organoids, matched stromal and immune cells and 3D tumor microenvironment models,” *BMC Cancer*, vol. 18, no. 1, p. 335, Mar. 2018, doi: 10.1186/s12885-018-4238-4.
- [7] G. Biffi and D. A. Tuveson, “Diversity and Biology of Cancer-Associated Fibroblasts,” *Physiol. Rev.*, vol. 101, no. 1, pp. 147–176, Jan. 2021, doi: 10.1152/physrev.00048.2019.
- [8] T. R. Wilson *et al.*, “Widespread potential for growth-factor-driven resistance to anticancer kinase inhibitors,” *Nature*, vol. 487, no. 7408, pp. 505–509, Jul. 2012, doi: 10.1038/nature11249.
- [9] H. Hu *et al.*, “Three subtypes of lung cancer fibroblasts define distinct therapeutic paradigms,” *Cancer Cell*, vol. 39, no. 11, pp. 1531-1547.e10, Nov. 2021, doi: 10.1016/j.ccell.2021.09.003.
- [10] M. Kim *et al.*, “Patient-derived lung cancer organoids as in vitro cancer models for therapeutic screening,” *Nat. Commun.*, vol. 10, no. 1, Art. no. 1, Sep. 2019, doi: 10.1038/s41467-019-11867-6.
- [11] S. Kim *et al.*, “Comparison of Cell and Organoid-Level Analysis of Patient-Derived 3D Organoids to Evaluate Tumor Cell Growth Dynamics and Drug Response,” *Slas Discov.*, vol. 25, no. 7, pp. 744–754, Aug. 2020, doi: 10.1177/2472555220915827.
- [12] M. Polymenis, “Proteins associated with the doubling time of the NCI-60 cancer cell lines,” *Cell Div.*, vol. 12, p. 6, Aug. 2017, doi: 10.1186/s13008-017-0032-y.
- [13] D. J. Holt, L. M. Chamberlain, and D. W. Grainger, “Cell–cell signaling in co-cultures of macrophages and fibroblasts,” *Biomaterials*, vol. 31, no. 36, pp. 9382–9394, Dec. 2010, doi: 10.1016/j.biomaterials.2010.07.101.
- [14] X. Luo *et al.*, “Hydrogel-based colorectal cancer organoid co-culture models,” *Acta Biomater.*, vol. 132, pp. 461–472, Sep. 2021, doi: 10.1016/j.actbio.2020.12.037.
- [15] H. Zhao, E. Jiang, and Z. Shang, “3D Co-culture of Cancer-Associated Fibroblast with Oral Cancer Organoids,” *J. Dent. Res.*, vol. 100, no. 2, pp. 201–208, Feb. 2021, doi: 10.1177/0022034520956614.
- [16] V. S. Atanasova *et al.*, “Mimicking tumor cell heterogeneity of colorectal cancer in a patient-derived organoid-fibroblast model,” *Cancer Biology*, preprint, Mar. 2022. doi: 10.1101/2022.03.07.483214.

- [17] J. Liu *et al.*, “Cancer-Associated Fibroblasts Provide a Stromal Niche for Liver Cancer Organoids That Confers Trophic Effects and Therapy Resistance,” *Cell. Mol. Gastroenterol. Hepatol.*, vol. 11, no. 2, pp. 407–431, 2021, doi: 10.1016/j.jcmgh.2020.09.003.
- [18] W. Wang *et al.*, “Crosstalk to Stromal Fibroblasts Induces Resistance of Lung Cancer to Epidermal Growth Factor Receptor Tyrosine Kinase Inhibitors,” *Clin. Cancer Res.*, vol. 15, no. 21, pp. 6630–6638, Nov. 2009, doi: 10.1158/1078-0432.CCR-09-1001.
- [19] M. Majety, L. P. Pradel, M. Gies, and C. H. Ries, “Fibroblasts Influence Survival and Therapeutic Response in a 3D Co-Culture Model,” *PLOS ONE*, vol. 10, no. 6, p. e0127948, Jun. 2015, doi: 10.1371/journal.pone.0127948.
- [20] D. Movia, D. Bazou, and A. Prina-Mello, “ALI multilayered co-cultures mimic biochemical mechanisms of the cancer cell-fibroblast cross-talk involved in NSCLC MultiDrug Resistance,” *BMC Cancer*, vol. 19, no. 1, p. 854, Aug. 2019, doi: 10.1186/s12885-019-6038-x.
- [21] S.-D. Jang *et al.*, “Anti-Cancer Activity Profiling of Chemotherapeutic Agents in 3D Co-Cultures of Pancreatic Tumor Spheroids with Cancer-Associated Fibroblasts and Macrophages,” *Cancers*, vol. 13, no. 23, p. 5955, Nov. 2021, doi: 10.3390/cancers13235955.
- [22] S.-Y. Jeong, J.-H. Lee, Y. Shin, S. Chung, and H.-J. Kuh, “Co-Culture of Tumor Spheroids and Fibroblasts in a Collagen Matrix-Incorporated Microfluidic Chip Mimics Reciprocal Activation in Solid Tumor Microenvironment,” *PLOS ONE*, vol. 11, no. 7, p. e0159013, Jul. 2016, doi: 10.1371/journal.pone.0159013.
- [23] A. Y. Hsiao *et al.*, “Microfluidic system for formation of PC-3 prostate cancer co-culture spheroids,” *Biomaterials*, vol. 30, no. 16, pp. 3020–3027, Jun. 2009, doi: 10.1016/j.biomaterials.2009.02.047.
- [24] H. Ma, T. Liu, J. Qin, and B. Lin, “Characterization of the interaction between fibroblasts and tumor cells on a microfluidic co-culture device,” *ELECTROPHORESIS*, vol. 31, no. 10, pp. 1599–1605, 2010, doi: 10.1002/elps.200900776.
- [25] L. Ewart *et al.*, “Performance assessment and economic analysis of a human Liver-Chip for predictive toxicology,” *Commun. Med.*, vol. 2, no. 1, Art. no. 1, Dec. 2022, doi: 10.1038/s43856-022-00209-1.
- [26] Q. Luan *et al.*, “Non-small cell lung carcinoma spheroid models in agarose microwells for drug response studies,” *Lab. Chip*, vol. 22, no. 12, pp. 2364–2375, 2022, doi: 10.1039/D2LC00244B.
- [27] X. Gong *et al.*, “Generation of Multicellular Tumor Spheroids with Microwell-Based Agarose Scaffolds for Drug Testing,” *PLOS ONE*, vol. 10, no. 6, p. e0130348, Jun. 2015, doi: 10.1371/journal.pone.0130348.
- [28] C. Eilenberger *et al.*, “A Microfluidic Multisize Spheroid Array for Multiparametric Screening of Anticancer Drugs and Blood–Brain Barrier Transport Properties,” *Adv. Sci.*, vol. 8, no. 11, p. 2004856, 2021, doi: 10.1002/advs.202004856.
- [29] K. Okamoto *et al.*, “Role of Survivin in EGFR Inhibitor–Induced Apoptosis in Non–Small Cell Lung Cancers Positive for EGFR Mutations,” *Cancer Res.*, vol. 70, no. 24, pp. 10402–10410, Dec. 2010, doi: 10.1158/0008-5472.CAN-10-2438.
- [30] C. for D. E. and Research, “FDA grants accelerated approval to adagrasib for KRAS G12C-mutated NSCLC,” *FDA*, Dec. 2022, Accessed: Jan. 03, 2023. [Online]. Available:

- <https://www.fda.gov/drugs/resources-information-approved-drugs/fda-grants-accelerated-approval-adagrasib-kras-g12c-mutated-nsclc>
- [31] Y. Li, X. Gao, C. Ni, B. Zhao, and X. Cheng, “The application of patient-derived organoid in the research of lung cancer,” *Cell. Oncol.*, Jan. 2023, doi: 10.1007/s13402-023-00771-3.
- [32] P. Fusco *et al.*, “Patient-derived organoids (PDOs) as a novel in vitro model for neuroblastoma tumours,” *BMC Cancer*, vol. 19, no. 1, p. 970, Oct. 2019, doi: 10.1186/s12885-019-6149-4.
- [33] R. J. Murphy, G. Gunasingh, N. K. Haass, and M. J. Simpson, “Growth and adaptation mechanisms of tumour spheroids with time-dependent oxygen availability.” bioRxiv, p. 2022.04.24.489294, Apr. 24, 2022. doi: 10.1101/2022.04.24.489294.
- [34] D. A. J. Gendre, E. Ameti, W. Karenovics, N. Perriraz-Mayer, F. Triponez, and V. Serre-Beinier, “Optimization of tumor spheroid model in mesothelioma and lung cancers and anti-cancer drug testing in H2052/484 spheroids,” *Oncotarget*, vol. 12, no. 24, pp. 2375–2387, Nov. 2021, doi: 10.18632/oncotarget.28134.
- [35] J. M. Ayuso *et al.*, “Organotypic microfluidic breast cancer model reveals starvation-induced spatial-temporal metabolic adaptations,” *eBioMedicine*, vol. 37, pp. 144–157, Nov. 2018, doi: 10.1016/j.ebiom.2018.10.046.
- [36] B. Arneth, “Tumor Microenvironment,” *Medicina (Mex.)*, vol. 56, no. 1, Art. no. 1, Jan. 2020, doi: 10.3390/medicina56010015.
- [37] L. Tao, G. Huang, H. Song, Y. Chen, and L. Chen, “Cancer associated fibroblasts: An essential role in the tumor microenvironment (Review),” *Oncol. Lett.*, vol. 14, no. 3, pp. 2611–2620, Sep. 2017, doi: 10.3892/ol.2017.6497.
- [38] M. Nguyen *et al.*, “Dissecting Effects of Anti-cancer Drugs and Cancer-Associated Fibroblasts by On-Chip Reconstitution of Immunocompetent Tumor Microenvironments,” *Cell Rep.*, vol. 25, no. 13, pp. 3884–3893.e3, Dec. 2018, doi: 10.1016/j.celrep.2018.12.015.
- [39] P. Liu *et al.*, “A bladder cancer microenvironment simulation system based on a microfluidic co-culture model,” *Oncotarget*, vol. 6, no. 35, pp. 37695–37705, Oct. 2015.
- [40] Q. Liu, T. Zhao, X. Wang, Z. Chen, Y. Hu, and X. Chen, “In Situ Vitriification of Lung Cancer Organoids on a Microwell Array,” *Micromachines*, vol. 12, no. 6, Art. no. 6, Jun. 2021, doi: 10.3390/mi12060624.
- [41] D. Choi *et al.*, “Microfluidic Organoid Cultures Derived from Pancreatic Cancer Biopsies for Personalized Testing of Chemotherapy and Immunotherapy,” *Adv. Sci.*, vol. n/a, no. n/a, p. 2303088, doi: 10.1002/advs.202303088.

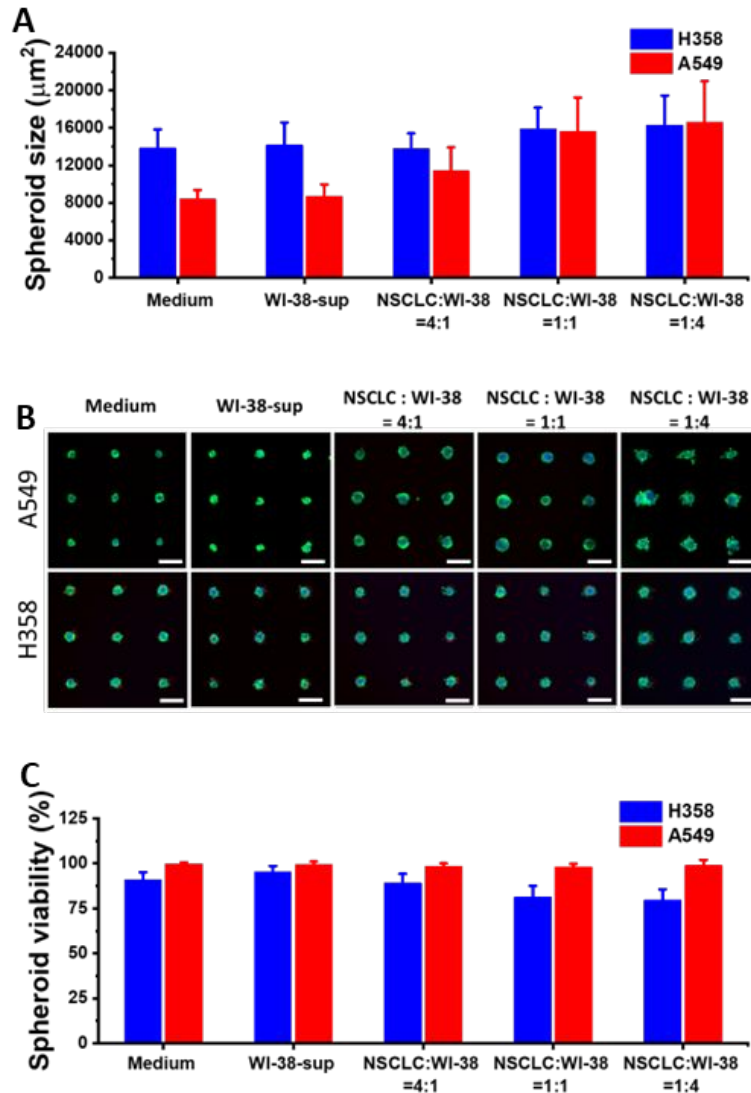


Figure 1. Co-culture spheroids for one week in agarose microwells. NSCLC cell lines A549 and NCI-H358 were co-cultured with fibroblast WI-38 and supernatant for 1 week and formed tight spheroids with high viability in agarose microwells. Spheroid size increased based on the increasing number of fibroblasts seeding with CV<30% (A). (B) Live/dead stain images of spheroids after 1-week culture. Live cells fluoresced bright green (Calcein AM), blue nucleus (Hoechst 33342) and dead cells fluoresced red (propidium iodide). The viability of A549 and WI-38 co-cultured spheroid was > 98%, and the viability of NCI-H358 and WI-38 co-cultured spheroid was >80% while NCI-H358 with WI-38 supernatant was >90% after 1-week incubation (C). Scale bar: 200μm.

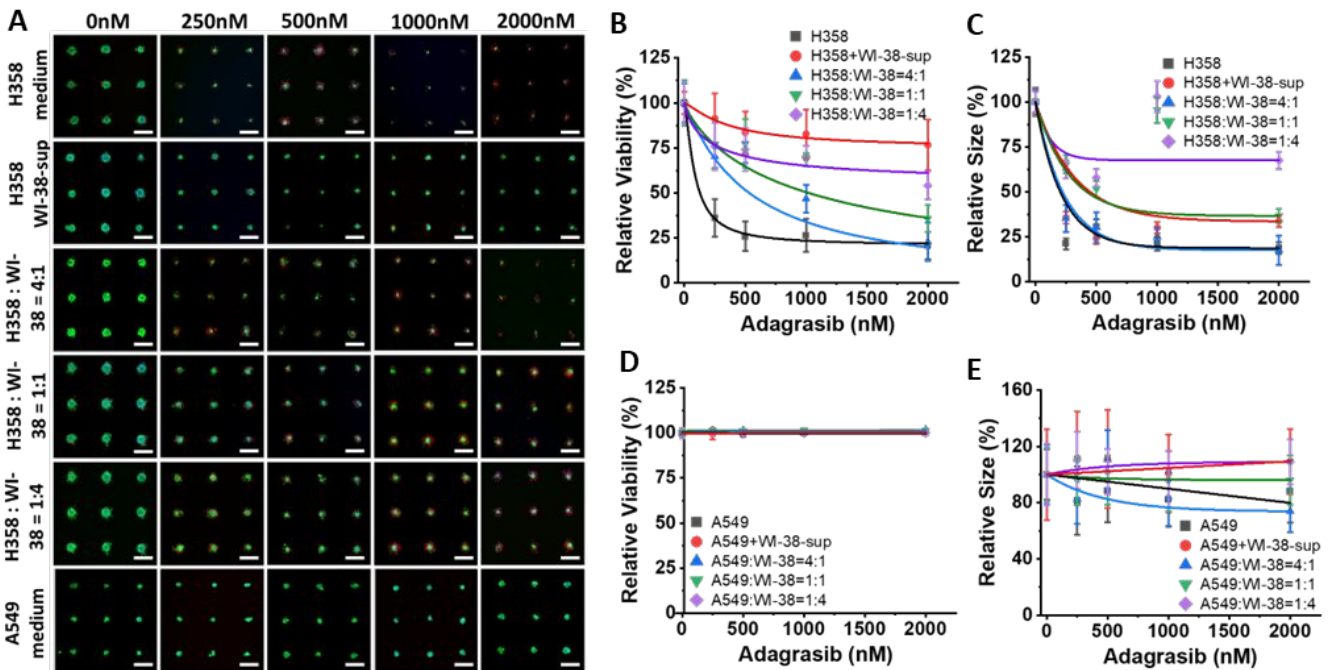


Figure 2. Cytotoxicity of spheroids in agarose microwells. NCI-H358 and WI-38 co-culture spheroids were exposed to adagrasib from 250nM to 2000nM (A), NCI-H358 cultured with WI-38 supernatant and WI-38 cells showed the drug resistance with higher viability (B) and spheroid size (C) under the adagrasib treatments. A549 with the wild-type KRAS^{G12C}, showed negative response to adagrasib in both cytotoxicity (D) and size assessment (E). Green: Calcein AM, red: Propidium iodide, blue: Hoechst. Scale bar: 200 μ m.

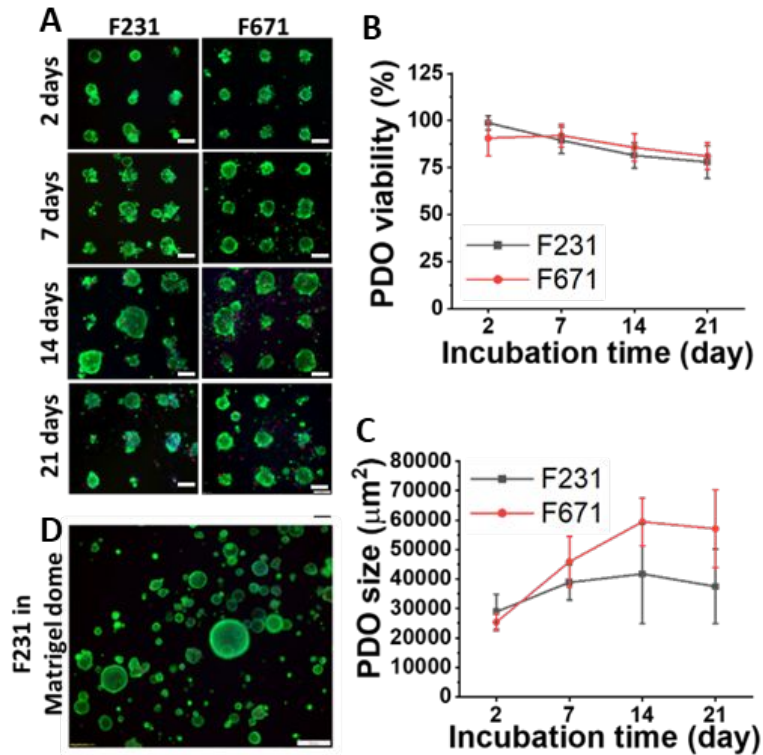


Figure 3. (A) Live/dead staining images of F231 and F671PDOs after 2 to 21 d culture. Green: Calcein AM, red: Propidium iodide, blue: Hoechst. Scale bar: 200 μm . (B) PDOs maintained the high viability ($>80\%$) in the first 2 weeks of incubation. (C) PDOs exhibit an initial trend of enlarging in size during the first two weeks of incubation, followed by a subsequent reduction in size attributable to decreased viability. (D) PDO F231 cultured in Matrigel dome showed high viability ($91.4\pm 11.6\%$) after 7 d but large CV of PDO size (126.38% , $n=3$). Scale bar: 500 μm .

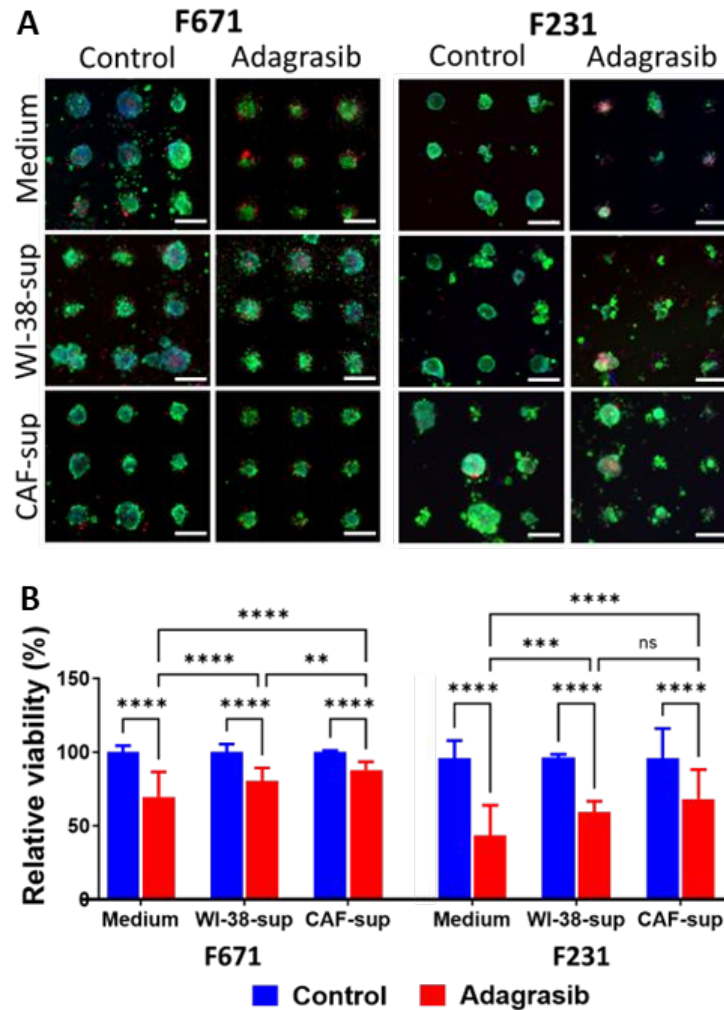


Figure 4. Cytotoxicity evaluation of F671 and F231 PDOs condition in normal medium and CAF 41 supernatant. Live/dead fluorescent images (A) and spheroid viability evaluation (B) showed F671 and F231 were sensitive to adagrasib (500 nM) and WI-38/CAF supernatant can increase the drug resistance. Scale bars: 300 μm . Two-ways ANOVA, $^{ns}p > 0.05$, $^{**}p < 0.01$, $^{***}p < 0.001$, $^{****}p < 0.0001$

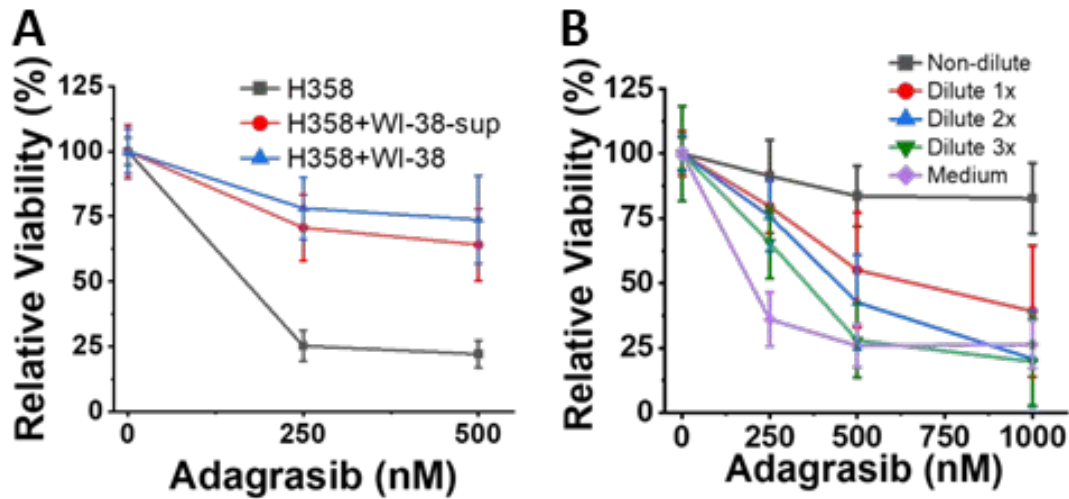


Figure 5. Evaluation of fibroblast supernatant contribution to drug resistance on NCI-H358 spheroid. Adagrasib showed similar cytotoxic effects on NCI-H358+WI-38 co-cultured spheroids and NCI-H358 spheroids under WI-38 supernatant (A). With the increasing dilution times of WI-38 supernatant, the drug resistance of NCI-H358 to adagrasib was decreasing (B), suggesting the secretion of WI-38 in supernatant helped to maintain NCI-H358 spheroids conditions during treatments.

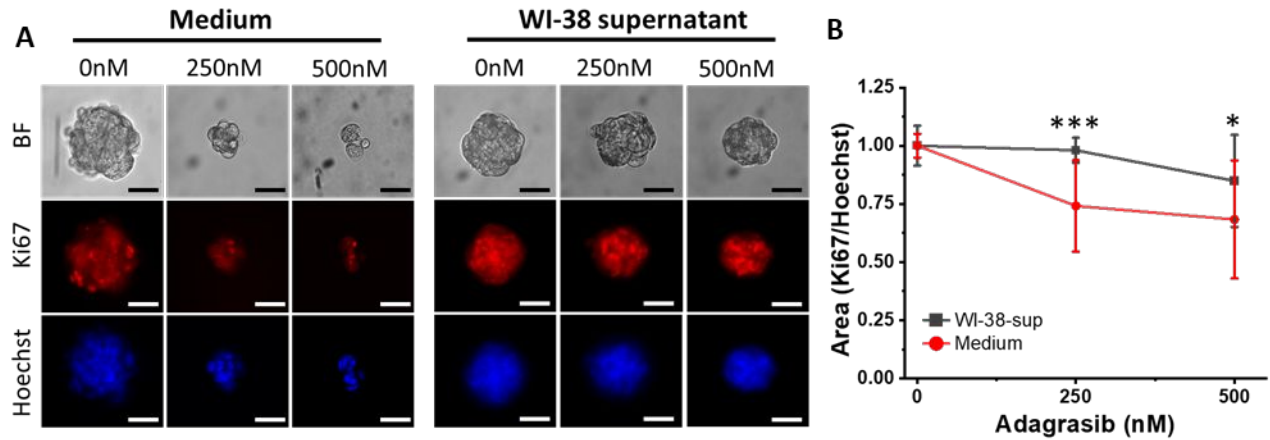


Figure 6. Contribution of fibroblast secretion on maintenance of cell proliferation. Ki67 as a proliferation biomarker was used to visualize the cells that maintained proliferation ability (A). scale bars: 50 μm . WI-38 supernatant maintained the higher Ki67/Hoechst ratio in NCI-H358 spheroids than normal culture medium after 48 h treatment (B). Two-sample t-test, *** $p < 0.001$, * $p < 0.05$.

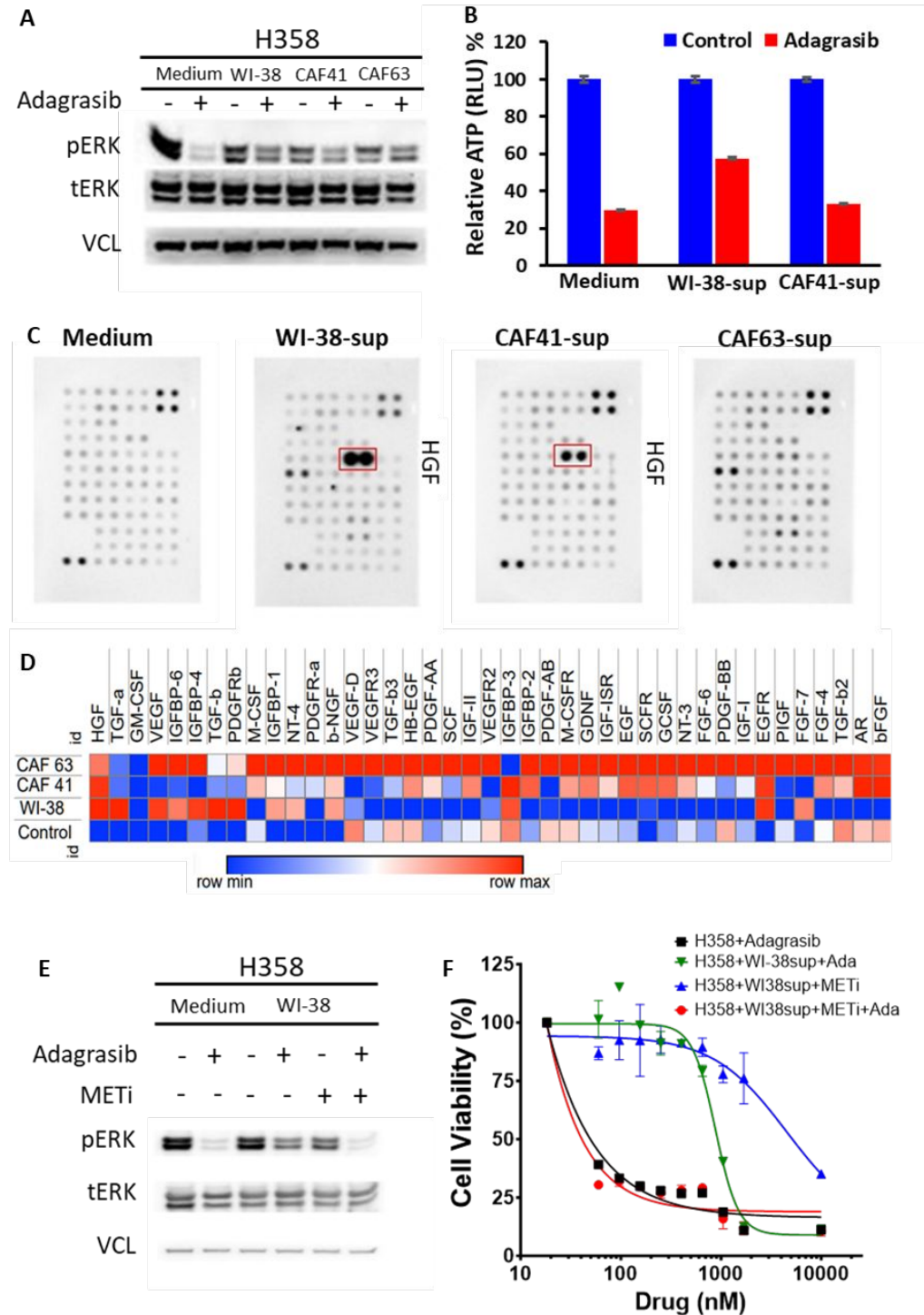


Figure 7. The effect of fibroblast supernatant on the maintenance of proliferative signals. Under the adagrasib treatment (500nM, 72h), all WI-38, CAF 41 and CAF 63 supernatants sustain pERK proliferation signal in different levels (A) that correlates with higher levels of ATP after adagrasib treatment (B). 41-growth factors in the supernatant of the studied fibroblasts (C, D) were evaluated by antibody array membrane. Finally, MET inhibitor cabozantinib counteracts the effect of sustaining pERK proliferation signals from fibroblast supernatant (E) and re-sensitizing cells to G12C inhibitors (F).